

Research Paper

# Investigating the Intracellular Behaviors of Liposomal Nanohybrids *via* SERS: Insights into the Influence of Metal Nanoparticles

Dan Zhu, Zhuyuan Wang<sup>✉</sup>, Shenfei Zong, Yizhi Zhang, Chen Chen, Ruohu Zhang, Binfeng Yun, Yiping Cui<sup>✉</sup>

Advanced Photonics Center, Southeast University, 2# Sipailou, Nanjing 210096, Jiangsu, China

✉ Corresponding author: cyp@seu.edu.cn, wangzy@seu.edu.cn

© Ivyspring International Publisher. This is an open access article distributed under the terms of the Creative Commons Attribution (CC BY-NC) license (<https://creativecommons.org/licenses/by-nc/4.0/>). See <http://ivyspring.com/terms> for full terms and conditions.

Received: 2017.05.24; Accepted: 2017.11.07; Published: 2018.01.01

## Abstract

The recent proposition to combine liposomes with nanoparticles presents great opportunities to develop multifunctional drug delivery platforms. Although impressive progress has been made, attempts to elucidate the role nanoparticles play in the integral nanohybrids are still rather limited. Here, using surface-enhanced Raman scattering (SERS) technique, we investigate the influence of metal nanoparticles on the liposomal properties, ranging from drug release to intracellular movement. Specifically, we prepared SERS-active nanohybrids by attaching metal nanoparticles to liposomes and employed SERS signals to explore the intracellular behavior of the nanohybrids. Once deposited on the cell membrane, the nanohybrids entered tumor cells *via* clathrin-mediated endocytosis and then moved to lysosomes. In comparison with pure liposomes, metal nanoparticles in the nanohybrids had little influence on the properties of liposomes. This study fills the gap of the function of nanoparticles in the overall nanohybrids, which provides a significant prerequisite for efficient drug delivery in therapeutic applications.

Key words: liposomes; metal nanoparticles; nanohybrids; SERS; intracellular behavior.

## Introduction

A number of recent developments in biomedical science concentrate on the design of efficient drug delivery systems (DDS) to deliver various therapeutic agents ranging from small molecule drugs to biomacromolecules (e.g., genes, proteins) [1-3]. Among these available approaches, liposomes have played an indispensable role due to their appealing nature including high biocompatibility, large drug carrying capacity and convenient and feasible tunability, which have attracted considerable attention in the field of drug delivery [4-6]. However, pure liposomes suffer from poor stability since they are prone to adhere and fuse to form larger ones in suspension [7]. Moreover, the fusion process may result in drug leakage, unexpected inclusion inactivation and inefficient delivery. Thus, nanoparticles have been introduced to stabilize liposomes in order to overcome the drug leakage

resulting from fusion or collapse [8-10]. To date, nanoparticles-functionalized liposomes, so called liposomal nanohybrids, have gradually been developed as theranostic nanoscale delivery systems [11-13]. Nanoparticles, such as iron oxides, quantum dots and metal nanoparticles, are recognized as offering extraordinary features for diagnostics as well as therapeutics [14, 15]. For example, Shin's group demonstrated that a gold cluster-labeled thermosensitive liposome is capable of triggering drug release in the tumor microenvironment by an external stimulation of NIR light, which improved the efficacy of therapy [16]. Similarly, Liu et al. prepared betulinic acid liposomes coated with a layer of gold nanoshell as a novel multifunctional nanodrug delivery system [17]. Their results verified that under NIR light irradiation, a synergetic efficacy of chemotherapy and photothermal therapy was

achieved successfully. Owing to its great clinical prospects, employing nanoparticle conjugation to implement remotely triggered drug release from liposomes is starting to prevail.

The interaction between nano hybrids and cells is always an important prerequisite for the successful delivery of therapeutics against various tumors. The application of nano hybrids in biomedicine requires a much deeper understanding of their endocytosis and intracellular behaviors. Early work carried out on the cellular uptake of nano hybrids have demonstrated that most nano hybrids, including liposome-quantum dot hybrids and magnetic liposomes, are taken up through an endocytic process and their uptake is time- and concentration-dependent [18, 19]. Additionally, investigations on the influence of quantum dots and superparamagnetic iron oxides were often overlooked in previous literature. Understanding whether nanoparticles impact the liposomal properties is highly important for their efficient delivery, which serves as their crucial role in cancer therapy. However, until now, there is little research focused on the role that nanoparticles play in the intracellular behavior of nano hybrids.

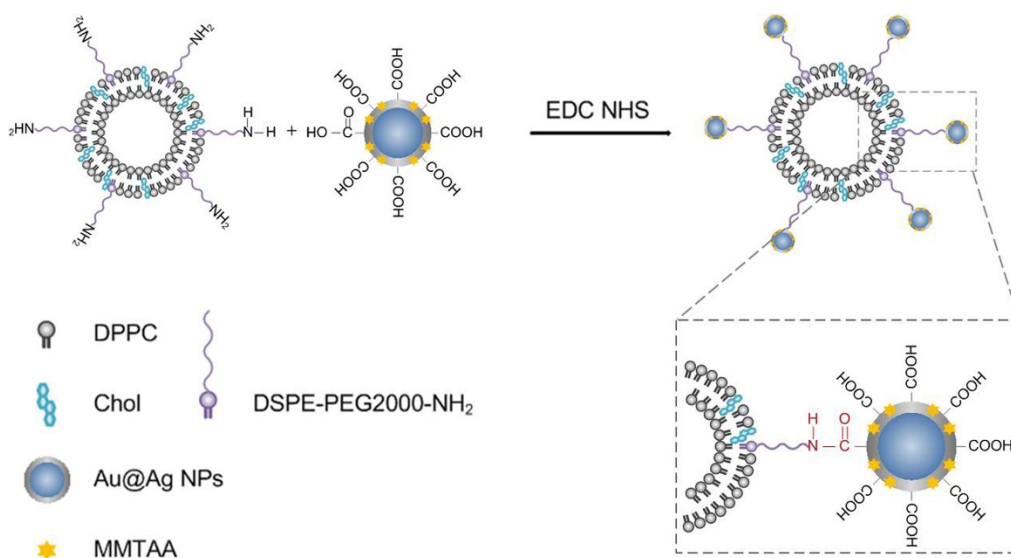
In the current study, using a SERS-based tracking method, we attempt to provide an insight into these relatively unexplored areas by systematically comparing the liposomal behaviors of liposomes conjugated with and without nanoparticles. In the experiments, a kind of metal-liposome nano hybrid was developed by covalently attaching gold/silver core-shell nanoparticles to thermally sensitive liposomes. In such a structure, 2-mercapto-4-methyl-5-thiazoleacetic acid (MMTAA) molecules are used as

both the Raman reporter for generating SERS signals and the conjugation linker for the subsequent attachment. Meanwhile, the metal nanoparticles serve as SERS substrates as well as the materials for enhancing the photothermal response. To investigate the endocytosis process and the intracellular fate of the nano hybrids, SERS signals were exploited for imaging their distributions in cells due to their high photostability and resistance to fluorescence interference. Further, in a comparable study with fluorophore-labeled liposomes, the impact of metal nanoparticles on liposomal behavior was analyzed. This study revealed a universal concept for the role nanoparticles play in nano hybrids, which would inspire the development and application of multifunctional drug nanocarriers based on liposomal nano hybrids.

## Results and Discussion

### Preparation and characterization

Scheme 1 depicts the general strategy for preparing the metal-liposome nano hybrids. The first step consists of the exchange of sodium citrate molecules from the Au@Ag core-shell nanoparticles with MMTAA molecules. In such a way, carboxyl-modified Au@Ag core-shell nanoparticles (Au@Ag@MMTAA) were obtained. Thereafter, the terminal carboxyl groups of the carboxylated nanoparticles were reacted with an amino-ended lipid (DSPE-PEG2000-NH<sub>2</sub>) contained in the liposomes, *via* amide conjugation. Finally, the liposomal nano hybrids were accomplished, which were stable in biological media.



**Scheme 1.** A sketch depicting the general strategy for the conjugation of the carboxyl-functionalized nanoparticles to liposomes containing an aminated lipid (DSPE-PEG2000-NH<sub>2</sub>).

Film hydration followed by bath sonication was chosen as the preferred method to prepare the amino-modified liposomes. Figure 1A reveals a representative TEM image of an individual liposome with an apparent hollow vesicle structure. The liposomes containing zwitterionic (DPPC) and cationic (DSPE-PEG2000-NH<sub>2</sub>) lipids exhibited an average diameter of 153.6 nm (Figure 1C) and a weak positive surface charge (+8.5 mV; Figure 1F). The role of DSPE-PEG2000-NH<sub>2</sub> is to provide a few amino anchor points on the outer surfaces of liposomes for the selective binding of the metal nanoparticles. As an additional advantage, the PEG-based chain increased the stability of liposomes in the high ionic strength cellular media, avoiding irreversible liposome fusion or aggregation [20, 21].

The Au@Ag@MMTAA nanoparticles presented a sole extinction peak at 400 nm, suggesting that no aggregation occurred during the decoration process [22]. As further confirmed by DLS shown in Figure S1, the surface grafting with MMTAA molecules had no observable influence on the morphology, size or zeta potential. Here, MMTAA molecules have two functions. First, MMTAA molecules served as conjugation agents for the specific binding of metal nanoparticles to liposomes. Second, MMTAA molecules grasped the metal nanoparticles through thiol groups and acted as Raman reporters, which could generate strong SERS signals. This dual-function molecule simplified the fabrication protocol.

In the next step, by incubating amino modified

vesicles with Au@Ag@MMTAA nanoparticles under identical conditions, nano hybrids with a medium loading capacity were obtained (Figure 1B). Specially, Au@Ag@MMTAA nanoparticles tend to intersperse as aggregates rather than individual nanoparticles. The distribution of the number of metal nanoparticles per nano hybrid was investigated by statistical analysis of TEM images (Figure S2). It showed that the coverage of Au@Ag@MMTAA nanoparticles on the liposomes varied from 10 nanoparticles per nano hybrid to 30 nanoparticles per nano hybrid. There were about 22 Au@Ag@MMTAA nanoparticles conjugated to one liposome on average. The binding of metal nanoparticles is chemically driven by the high affinity of the carboxyl terminal groups on the nanoparticle surfaces towards the amino-ended lipid in the vesicles, resulting in a slight growth in the size of liposomal nano hybrids (215.5 nm) and a switch in zeta potential (-11.6 mV) (Figure 1D and 1F). Additionally, the successful conjugation of metal nanoparticles on liposomes made the surface plasmon resonant band red-shift to 437 nm (Figure 1E), consistent with the color change from translucent white to misty brown. The red-shift of the surface plasmon resonant band after conjugation of metal nanoparticles to liposomes was reasonable since the Au@Ag nanoparticles attached to the lipid bilayers experienced a higher refractive index [23]. Meanwhile, the Au@Ag nanoparticles became closer to each other under this hybrid structure, resulting in the coupling of their SPR and thus the red-shift of the band [24].

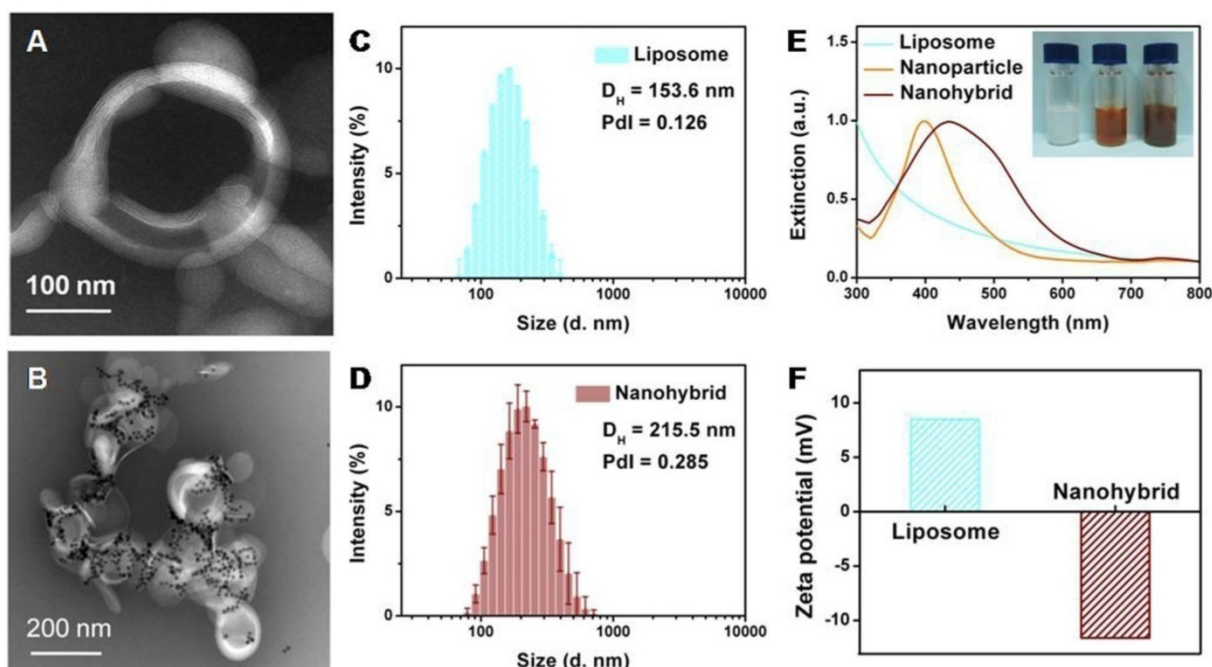


**Figure 1.** Characterization of liposomes and nano hybrids: TEM micrograph of liposomes (A) and nano hybrids (B); size distribution of liposomes (C) and nano hybrids (D); extinction spectra and photographs of solutions (E); surface zeta potential (F).

By contrast, liposome-metal nano hybrids with low coverage were also prepared by decreasing the number of Au@Ag nanoparticles involved in the reaction. Characterization confirmed that few nanoparticles were attached to the surface of the liposomes. Due to their low coverage by the metal nanoparticles, the obtained nano hybrids exhibited a small decline in zeta potential (+8.07 mV) and a slight red-shift of surface plasmon resonant peak (414 nm, Figure S3). The average size of nano hybrids measured by DLS was 328.2 nm. The reason for the growth may be that nanoparticles stuck neighboring liposomes together, which formed mild aggregates. The distribution of nanoparticle number per nano hybrid was also analysed and four Au@Ag@MMTAA nanoparticles were modified per lipid vesicle on average. Since nano hybrids with different surface coverage of nanoparticles were successfully fabricated, the conjugated nano-lipid hybrids showed good controllability, which was significant for further applications.

### Drug release kinetics

As a thermally sensitive lipid, DPPC molecules were incorporated into the lipid mixture in order to prepare temperature-responsive liposomes, whose phase pretransition and main-transition temperatures are around 35 °C and 41 °C, respectively [25]. To evaluate the release characteristics, anticancer drug, DOX, was encapsulated into the aqueous core through the pH gradient method [26]. The encapsulation efficiency was characterized by fluorescence spectroscopy, which confirmed a relatively high value of >90%. The thermal response of the liposomes and nano hybrids was studied by quantifying the amount of DOX released at 25, 37 and 43 °C (Figure 2). At room temperature (25 °C), no significant leakage of DOX from liposomes or nano hybrids was observed after 24 h. Both the liposomes and nano hybrids displayed a limited degree of DOX release at physiological temperature (37 °C). When ambient temperature exceeded the phase transition temperature (43 °C), rapid and intensive release of DOX from the liposomes and nano hybrids was discovered. This discharge of DOX was probably facilitated by the increased bilayer permeability at a higher temperature. On closer inspection, it was incontrovertible that they both demonstrated similar temperature-dependent characteristics. In other words, the conjugation of metal nanoparticles had no influence on the DOX release behavior from vesicles.

Metal nanoparticles are particularly promising materials for photothermal response, and are often applied for light-controllable drug release. Actually,

metal nanoparticles-modified liposomes maintained the photothermal effect. According to the plasmon resonant peak of nano hybrids, a NIR laser at 808 nm was selected in order to achieve two-photon adsorption. A comparative trial was conducted, in which we monitored drug release from liposomes and nano hybrids under laser stimulation. As shown in Figure S4, pure liposomes exhibited minimal drug leakage, indicating that they were not sensitive to the light stimuli. In contrast, the nano hybrids discharged nearly a quarter of the DOX molecules, which was five times greater than for liposomes without nanoparticles. This distinction can be explained by the influence of metal nanoparticles. Au@Ag@MMTAA nanoparticles on the surfaces of the liposomes transformed energy from the laser into heat, leading to destabilization of the lipid membranes and burst drug release [27]. In spite of the thermal response, the existence of metal nanoparticles endowed liposomes with another light response. This remote operation is a major reason for its popularity, which is a significant step in nanomedicine development.

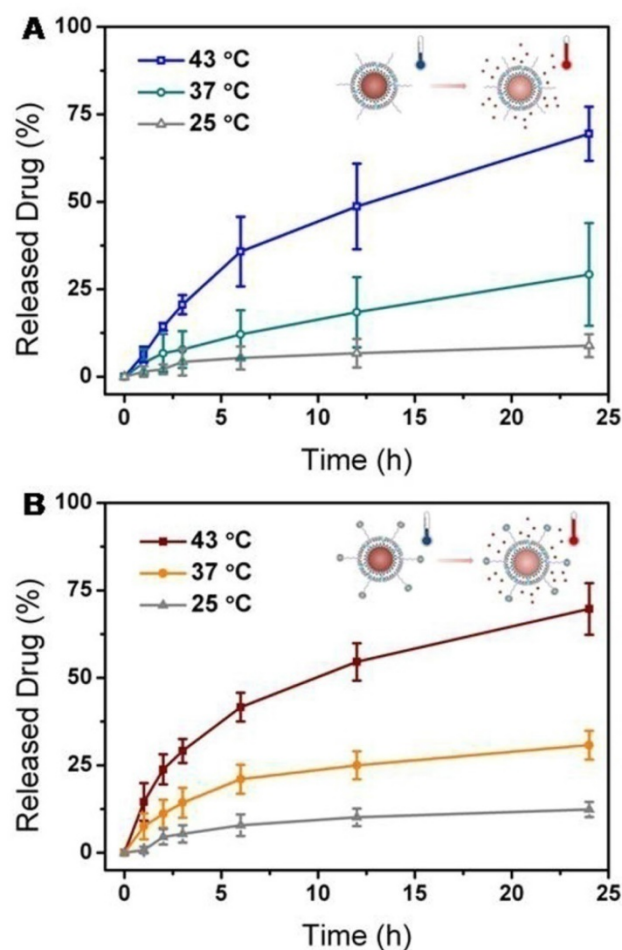


**Figure 2.** Drug release profiles of liposomes (A) and nano hybrids (B) at different temperatures: 25 °C, 37 °C and 43 °C.

## SERS Performance

Additionally, MMTAA molecules were employed as Raman reporters, whose characteristic spectrum is shown in Figure S5. Briefly, the most prominent Raman mode of MMTAA was the mode at  $1285\text{ cm}^{-1}$ , assigned to the CH in-plane bend mode [28, 29]. The SERS spectral characteristic of the nanohybrids was almost the same as the fingerprint signature of MMTAA, which suggested good maintenance during conjugation [30]. The enhancement factor (EF) of Au@Ag@MMTAA nanoparticles and nanohybrids were calculated to be  $1.08 \times 10^6$  and  $7.24 \times 10^5$ , respectively, which indicated that the introduction of liposomes did not affect the SERS activity of Au@Ag nanoparticles. Consequently, MMTAA molecules are capable of this double duty. The as-prepared nanohybrids were further applied to *in vitro* studies. SKBR3 cells were incubated with SERS-active nanohybrids and robust SERS signal was detected to track their location inside tumor cells. As shown in Figure 3, most of the nanohybrids were incorporated within cell membranes, while the rest entered the tumor cells. SERS images at different depths of SKBR3 cells were acquired to better prove this opinion (Figure S6). It was worth noting that no cell shape change or number reduction was observed, implying the outstanding biocompatibility of the nanohybrids.

## Stability study

Liposomal nanohybrids are expected to keep their morphology and property before their entry into cells. The nanohybrids preserved their hydrodynamic diameter and adsorption band after dispersion in PBS for 24 h, which indicated that the nanohybrids were quite stable in the buffer environment (Figure S7). However, liposomes usually suffer from aggregation in complex fluids, such as culture media, which would probably compromise their cellular entry. Thus, it is significant to probe the colloidal stability of nanohybrids in culture media of SKBR3 cells. After incubation with serum-free 1640 media for 12 h, the hydrodynamic diameter and adsorption band of nanohybrids underwent a slight increase and red-shift, respectively (Figure 4A and 4B). Inevitable adsorption of amino acids or proteins in the culture media was probably responsible for this [31, 32]. It has been considered that nanoparticle decoration and PEGylation could enhance their stability [33]. As a result, the nanohybrids demonstrated excellent stability in 1640 media over 12 h and suffered from minor aggregation.

After being taken up by SKBR3 cells, nanohybrids were tracked through their SERS signals.

These experiments were predicated on the assumption that no dissociation between nanoparticles and lipids occurred, especially at long time points. We wished to further visualize whether the intracellular environment may cleave nanoparticles from lipids. To achieve this goal, liposomes and metal nanoparticles were labeled with fluorescence and SERS agents, respectively. Using these two signals, we tracked liposomes and metal nanoparticles independently. The colocalization coefficient between SERS signals from nanoparticles and fluorescence signals from liposomes was utilized to analyze the stability of nanohybrids inside tumor cells. Here, the fluorescent dye, DiI, was chosen to mark liposomes because of its low cytotoxicity and transitivity. Since it tends to gather within lipid bilayers, DiI serves as a reasonable proxy for this test. The photoswitching behavior of DiI was used to realize super resolution imaging of the nanohybrids. Due to the excellent spatial resolution of PALM, the acquired image provided more direct evidence for the structural integrity of the nanohybrids. According to the super resolution imaging, no structure destruction was observed from the dual-labeled nanohybrids (Figure 5). We treated SKBR3 cells with nanohybrids and then imaged them at different time points. Confocal microscopy showed that the nanohybrids remained largely intact for the first 4 h, as evidenced in Figure 6. The intensity of SERS signals decreased with the culture time, as well as that of fluorescence signals. This reduction was likely due to metabolism of the nanohybrids by cells. To explore whether the nanohybrids were metabolized by cells through exocytosis, we co-incubated the nanohybrids with SKBR3 cells for different time. As shown in Figure S8, the content of nanohybrids within SKBR3 cells increased as a function of time in the first 8 h and reached a plateau afterwards. This can be explained by the equilibrium state between endocytosis and exocytosis, which also confirmed our hypothesis. After nanohybrids-loaded SKBR3 cells were supplemented with fresh culture medium, exocytosis prevailed gradually, leading to a decrease in the content of nanohybrids within SKBR3 cells as well as a reduction in the intensity of SERS signal. It is important to note that although the signal intensity suffered from a sharp decline, the contact ratio underwent a slight contraction, which was maintained at  $\sim 0.6$ . It can be asserted that negligible separation occurred after 12 h incubation. Thus, owing to their high stability *in vitro*, nanohybrids can be tracked by SERS signals generated from their metal nanoparticles after being taken up by SKBR3 cells.

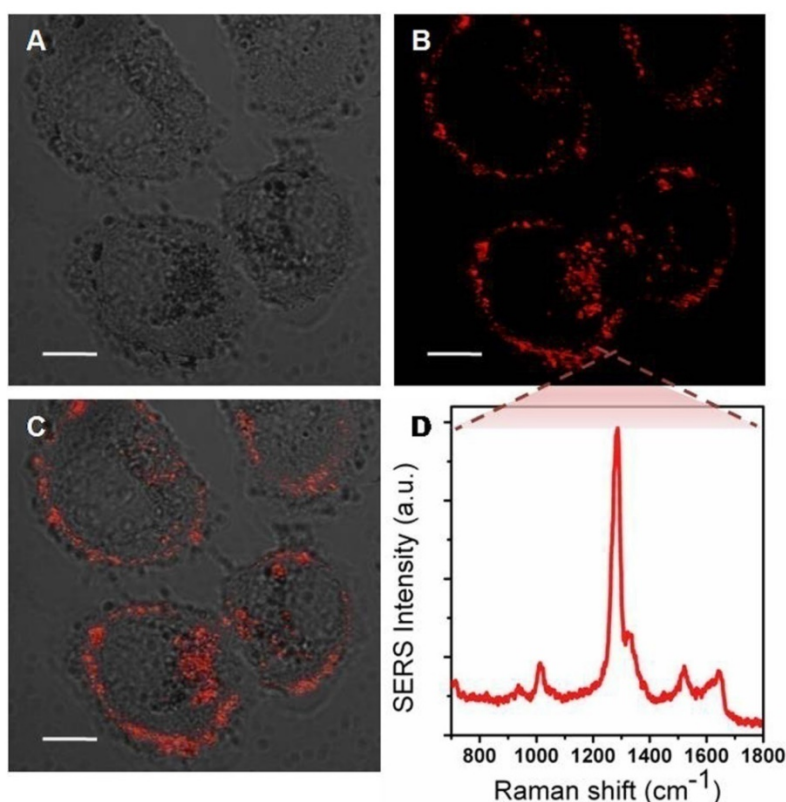


**Figure 3.** Bright field image (A), SERS mapping (B) and merged image (C) of SKBR3 cells incubated with nano hybrids for 5 h. (D) SERS spectrum acquired from the SKBR3 cells. Scale bars for confocal images are 10  $\mu\text{m}$ .

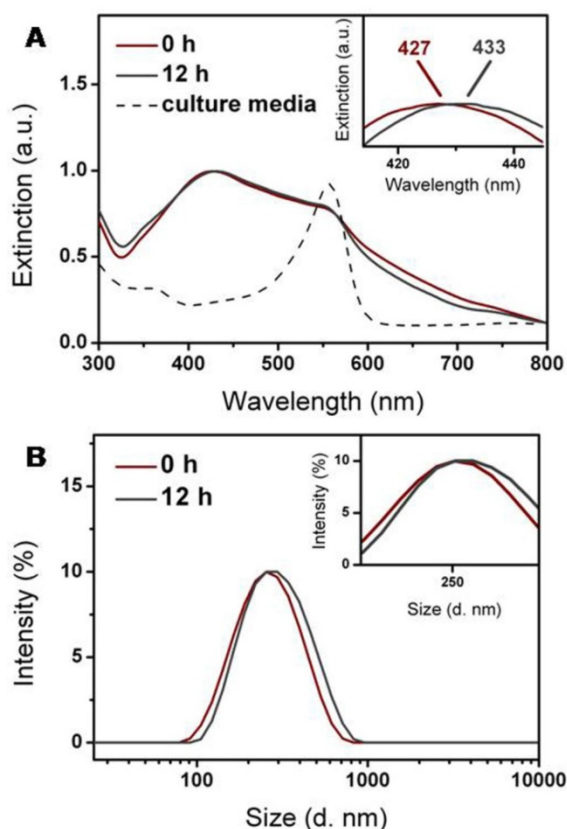


**Figure 4.** Colloidal stability of nano hybrids during incubation at 37 °C for 12 h in serum-free 1640 culture media. Nano hybrids displayed no apparent change in (A) extinction property and (B) size distribution.

### Cellular uptake and intracellular fate

Understanding the key internalization pathways of nano hybrids would form the basis of effective delivery. Generally, extracellular nanomaterials are taken up by tumor cells through endocytosis, which can be subdivided into phagocytosis for larger foreign materials and pinocytosis for smaller ones [34]. According to the different participating proteins, pinocytosis can be classified into three subcategories: clathrin-mediated endocytosis, caveolae-mediated endocytosis and micropinocytosis [35]. It was established that nano hybrids enter cells through pinocytosis. However, the exact mechanism remains variable under different situations. Here, SERS signals were acquired to evaluate the specific endocytosis pathway by which nano hybrids enter SKBR3 cells. First, SKBR3 cells were treated with three different inhibitors: namely chlorpromazine (clathrin inhibitor), nystatin (caveolae inhibitor) or cytochalasin D (actin inhibitor). Furthermore, the cells pretreated at 4 °C and the cells without inhibitor pretreatment under the same experimental conditions were studied as negative and positive control, respectively. Afterwards, the pretreated cells were incubated with SERS-active nano hybrids for 4 h. Eventually, cells with different treatments were washed and observed under a confocal laser scanning

microscope. In the positive control experiment, most of the cells showed a remarkable SERS activity with unambiguous and intense distribution (Figure 7A). Meanwhile, SERS punctuates were hardly visible when the experiment was performed at 4 °C (Figure 7B). Endocytosis is an energy dependent process, which would be inhibited at low temperature. As a result, nano hybrids got into SKBR3 cells *via* energy dependent endocytosis. In comparison, a significant reduction of cellular internalization of nano hybrids was observed in SKBR3 cells pretreated with chlorpromazine (Figure 7C). Additionally, nystatin treatment suppressed the uptake of nano hybrids somewhat, which indicated that caveolae-mediated endocytosis did not play a role in uptake of the nano hybrids (Figure 7D) [36]. Similarly, the uptake efficiency slightly diminished in SKBR3 cells blocked with cytochalasin D (Figure 7E). Therefore, the internalization process of nano hybrids is strongly dependent on energy, with clathrin-mediated endocytosis dominant and macropinocytosis less involved (Figure 7F).

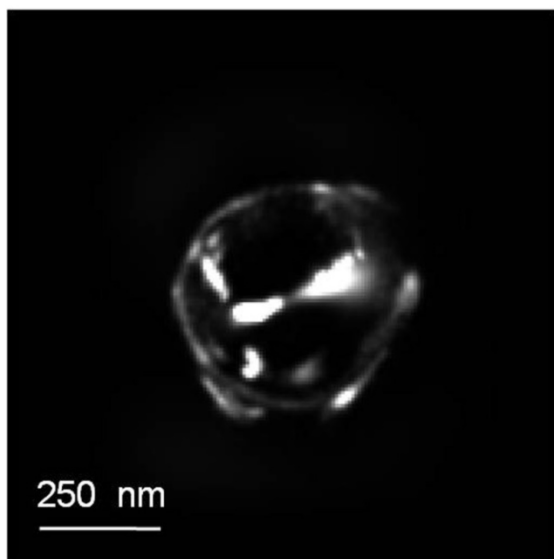


**Figure 5.** Super resolution image of SERS-fluorescence dual labeled nano hybrids.

It has been reported that nanomaterials entering cells through clathrin-mediated endocytosis are often transported to lysosomes. The intracellular behavior of nano hybrids was further investigated after cellular entry. To explore the intracellular fate of nano hybrids, specific fluorescence markers were utilized to stain intracellular compartments inside SKBR3 cells. These markers consisted of lyso-tracker (lysosomes) and DiI (membranes), respectively. By examining whether the SERS signals of nano hybrids colocalized with the stained subcellular organelles, we were able to

delineate the intracellular fate of the nano hybrids. The nano hybrids showed primarily colocalization with membranes after an incubation of 4 h (Figure 8A). This moderate association fell continuously over the entire incubation period of 12 h. Conversely, strong colocalization of nano hybrids with lysosomes was observed after 12 h. During the incubation time, signal intensity, as well as colocalization between nano hybrids and membranes, declined slightly. By contrast, colocalization between nano hybrids and lysosomes rose slowly. From these data, we concluded that the nano hybrids largely reside within lysosomes after their departure from cell membranes, consistent with the typical route of the endolysosomal pathway for the degradation of biological entities.

To understand how the metal nanoparticles influenced the intracellular behaviors of nano hybrids, we investigated the intracellular fate of pure liposomes alone (Figure 9). In the experiment, fluorescent lipid (PE-NBD) was added into the lipid mixture in order to obtain fluorescent NBD-liposomes. Characterization of NBD-liposomes suggested similarity with the former ones in each respect (Figure S9). Actually, the intracellular behavior of pure liposomes (adhesion to the cell surface and then endocytosis) was quite consistent with that of nano hybrids. Experimentally, strong colocalization of liposomes with membranes persisted during the whole incubation time, which might be caused by the strong affinity of lipid molecules between cell membranes and liposomes. In addition, the intracellular fluorescence intensity of liposomes became increasingly weak as a function of incubation time, indicating the possibility of intracellular degradation of liposomes. Despite these similar trends, nano hybrids suffered from intracellular degradation at a slower rate. In other words, compared with pure liposomes, nano hybrids had more prolonged retention inside SKBR3 cells.

We hypothesize that the metal nanoparticles were responsible for the tiny difference in the intracellular behaviors between liposomes and nano hybrids. To test this hypothesis, the intracellular locations of Au@Ag@MMTAA nanoparticles were investigated. As shown in Figure S10, pure metal nanoparticles exhibited almost exactly the same behavioral characteristics as nano hybrids. Both their retention time and distribution in subcellular organelles converged toward the same conclusion. Following the above experimental data, we come to the conclusion that Au@Ag@MMTAA nanoparticles had little influence on liposomal behaviors, ranging from drug release to intracellular movement. This insight into the role metal nanoparticles play in the whole nano hybrids would remove obstacles in the

programmable design of multifunction nanocarriers. It is reasonable to expect that liposomes modified with other metal nanoparticles (e.g., gold nanoshells) also abide by the same law. This universal rule, which

is not restricted to the nanostructures given in this study, is very practical in multifunctional drug delivery systems.

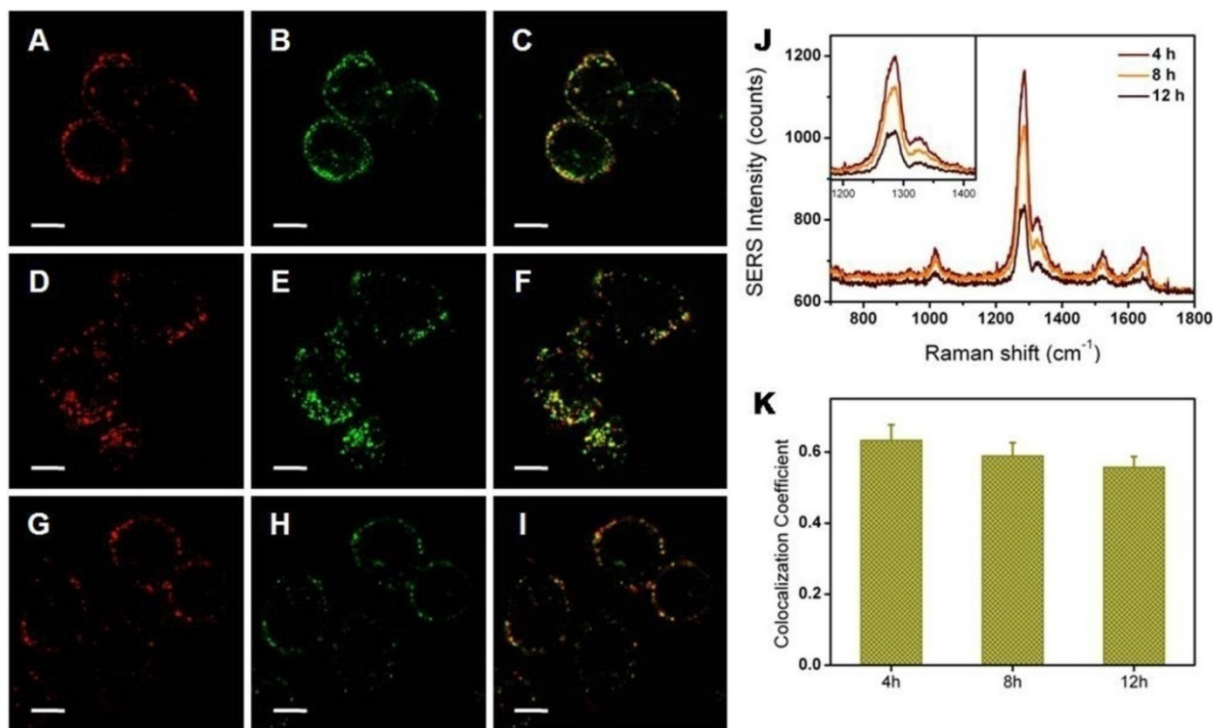


**Figure 6.** Colocalization between nanoparticles (labeled by SERS, red) and lipid bilayers (labeled by fluorescence, green) for 4 h (A-C), 8 h (D-F) and 12 h (G-I); 580-610 nm light was collected for fluorescence imaging of Dil and 800-1600  $\text{cm}^{-1}$  Raman scattered light was collected for SERS imaging. (J) Average SERS spectrum of a single SKBR3 cell incubated with the nano hybrids for different times. (K) Colocalization quantification (>0.6 indicates substantial colocalization). Scale bars for confocal images are 10  $\mu\text{m}$ .

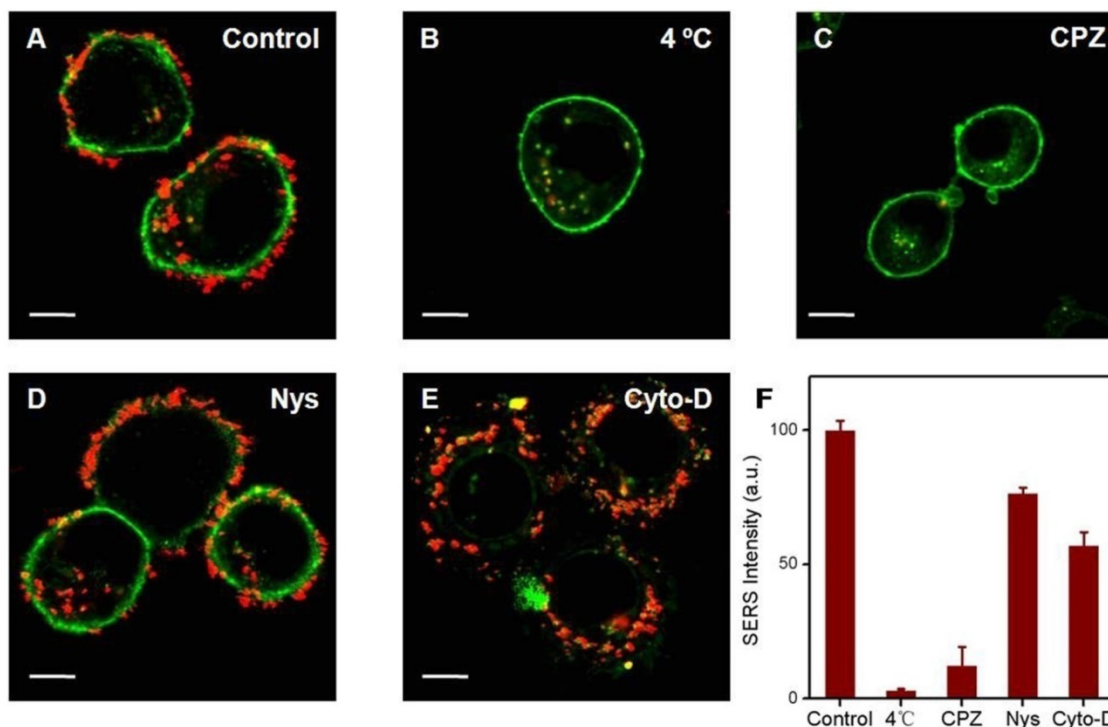


**Figure 7.** Effect of inhibitors on uptake of SKBR3 cells incubated with nano hybrids probed by SERS. In the intracellular experiments, 580-610 nm light was collected for fluorescence imaging of Dil (green) and 800-1600  $\text{cm}^{-1}$  Raman scattered light was collected for SERS imaging (red). Scale bars for confocal images are 10  $\mu\text{m}$ .

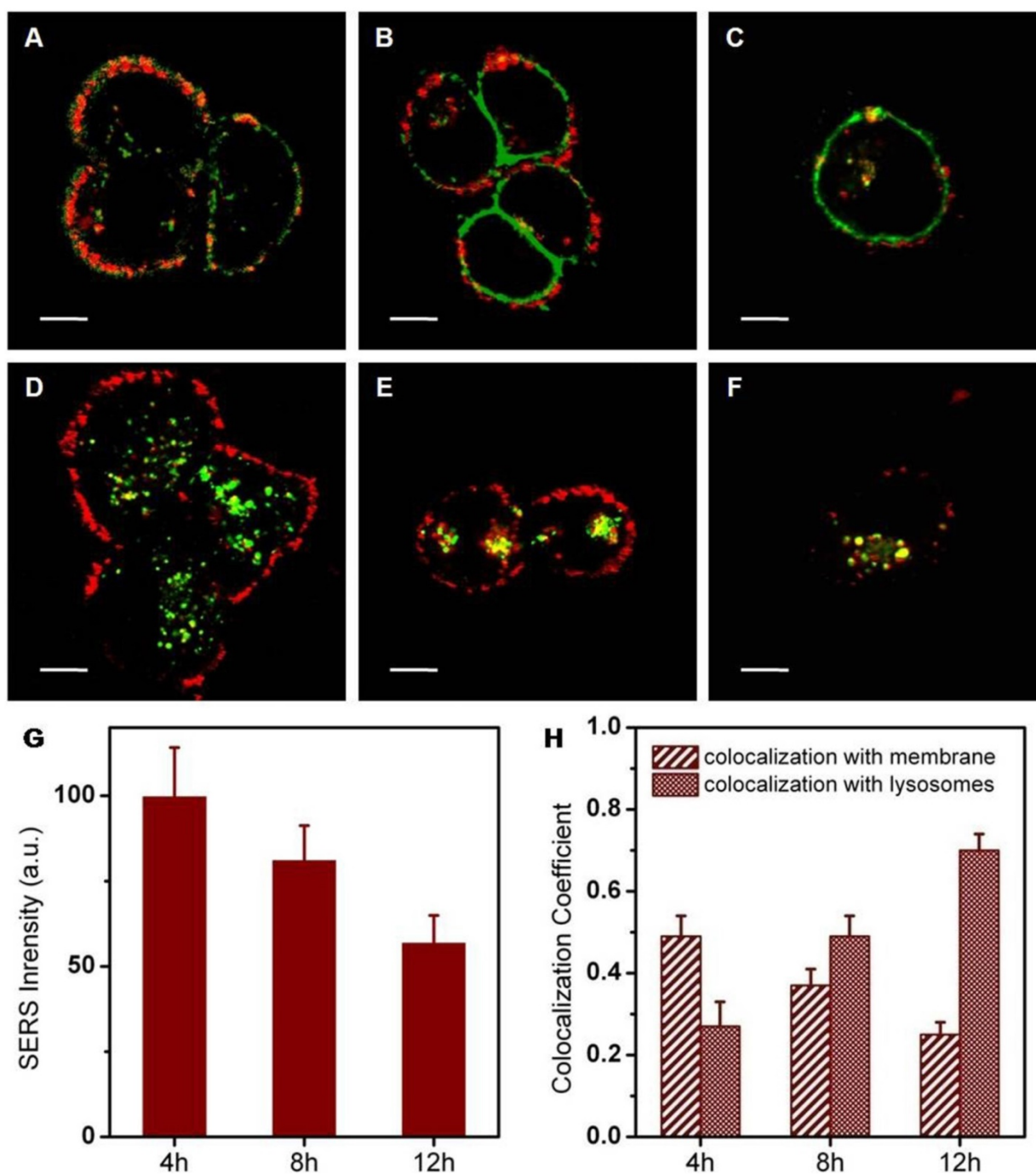


**Figure 8.** Confocal microscopy of SERS labeled nanohybrids (red) and fluorescence staining of organelle markers (green). Makers are Dil (membranes, A-C) and lyso-tracker green (lysosomes, D-F); 500-540 nm light was collected for the fluorescence imaging of LysoTracker Green, 580-610 nm light was collected for fluorescence imaging of Dil and 800-1600  $\text{cm}^{-1}$  Raman scattered light was collected for SERS imaging. (G) Average SERS intensity of a single SKBR3 cell incubated with the nanohybrids for 4, 8 and 12 h. (H) Colocalization coefficients between nanohybrids and membranes (or lysosomes). Scale bars for confocal images are 10  $\mu\text{m}$ .

In the end, we assessed the *in vitro* photothermal efficacy using confocal microscopy. As shown in Figure S11A, before laser irradiation, SKBR3 cells loaded with DOX/nanohybrids released little DOX, which showed weak fluorescence. After laser activation, DOX molecules were released to a great measure and exhibited strong fluorescence (Figure S11B). This phenomenon disclosed that photothermal

conversion led to tremendous drug release. It was notable that cells incubated with DOX/nanohybrids after the irradiation of laser had the lowest viability (Figure S11D). The NIR light would cause no cell damage when used alone. Therefore, the combined therapy was more efficient in killing tumor cells compared to solo treatment.

## Conclusion

This work demonstrated the successful preparation of nanohybrids based on thermally sensitive liposomes and gold/silver core-shell nanoparticles, which possessed excellent stability in the physiological environment. Efficient drug release from nanohybrids can be activated by bulk-heating or remote laser illumination. Cell experiments revealed that the nanohybrids entered SKBR3 cells mainly through clathrin-mediated endocytosis and tended to attach on the cell surface before arriving in acidic lysosomes. Additionally, SKBR3 cells loaded with

DOX/nanohybrids held the highest mortality *in vitro* after laser treatment. No obvious differences were observed between nanohybrids and liposomes, ranging from drug release to intracellular behaviors. According to this consequence, we infer a universal rule that metal nanoparticles undertake specific functions in the hybrid system but have little influence on liposomal behavior. Providing insights into the role that nanoparticles play in liposomal nanohybrid systems closely concerned with the modular design of functional nanocarriers, which would further facilitate their therapeutic effect in clinical applications.

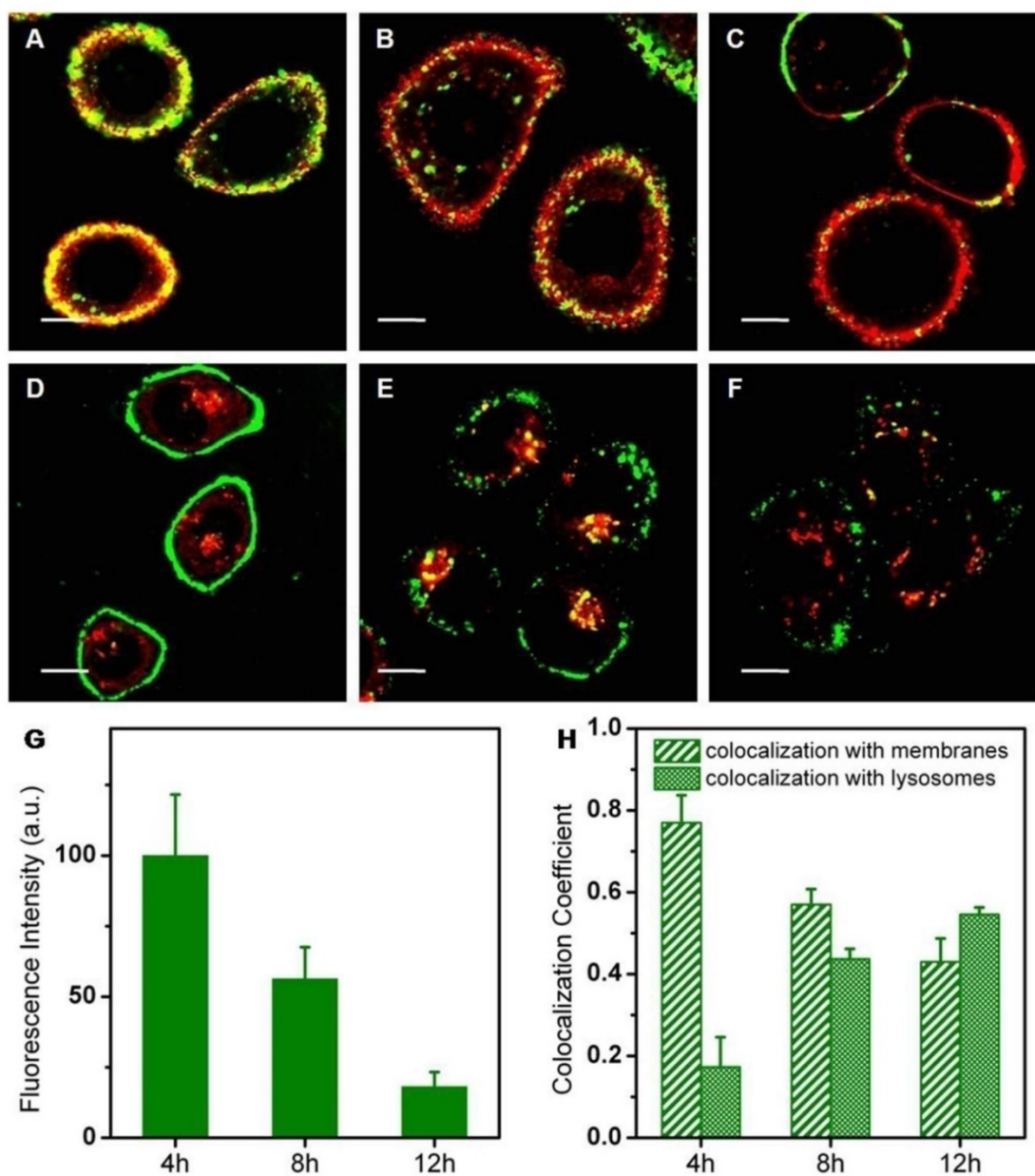


**Figure 9.** Confocal microscopy of NBD labeled liposomes (green) and fluorescence staining of organelle markers (red). Markers are Dil (membranes, A-C) and lysotracker red (lysosomes, D-F): 520-550 nm light was collected for fluorescence imaging of NBD, 580-610 nm light was collected for fluorescence imaging of Dil and 570-620 nm light was collected for fluorescence imaging of LysoTracker Red. (G) Average fluorescence intensity of a single SKBR3 cell incubated with the nanohybrids for 4, 8 and 12 h. (H) Colocalization coefficients between liposomes and membranes (or lysosomes). Scale bars for confocal images are 10  $\mu$ m.

## Materials and Methods

### Materials

1,2-dipalmitoyl-*sn*-glycero-3-phosphocholine (DPPC), 1,2-distearoyl-*sn*-glycero-3-phosphoethanolamine-N-[amino(polyethyleneglycol)-2000] (ammonium salt) (DSPE-PEG2000-NH<sub>2</sub>) and 1,2-dipalmitoyl-*sn*-glycero-3-phosphoethanolamine-N-(7-nitro-2-1,3-benzoxadiazol-4-yl) (ammonium salt) (PE-NBD) were purchased from Avanti Polar Lipids, USA. Cholesterol (Chol), hydrogen tetrachloroaurate (III) trihydrate (HAuCl<sub>4</sub>·3H<sub>2</sub>O) and silver nitrate (AgNO<sub>3</sub>) were purchased from Alfa Aesar. Doxorubicin (DOX), 1-ethyl-3-(3-dimethylaminopropyl)carbodiimide (EDC), N-hydroxysuccinimide (NHS) and 2-mercapto-4-methyl-5-thiazoleacetic acid (MMTAA) were purchased from Sigma Aldrich. Methanol, chloroform and Triton X-100 were purchased from Aladdin Reagent Co., Ltd. Trisodium citrate (Na<sub>3</sub>C<sub>6</sub>H<sub>5</sub>O<sub>7</sub>·2H<sub>2</sub>O) was purchased from Sinopharm Chemical Reagent Co., Ltd. Phosphate buffered saline (PBS, 10mM, pH 7.4) was purchased from Nanjing KeyGen Biotechnology Co., Ltd. All the reagents were used as received. Deionized water (Millipore Milli-Q grade) with a resistivity of 18.2 MΩ cm<sup>-1</sup> was used in all the experiments.

### Characterization

UV-vis absorption spectra were collected using a Shimadzu UV-3600 PC spectrophotometer with quartz cuvettes of 1 cm path length. Transmission electron microscopy (TEM) images were obtained with an FEI Tecnai G<sup>2</sup>T20 electron microscope operating at 200 kV. Dynamic light scattering (DLS) measurements and zeta potential experiments were performed using a Malvern Zetasizer Nano ZS 90. Photoluminescence emission spectra were recorded on an Edinburgh FLS920 spectrofluorometer. SERS measurements were performed with a confocal microscope (FV 1000, Olympus) equipped with a spectrograph (Sharmrock SR-303i-A, Andor) with a Newton charge-couple device (CCD). He-Ne laser with 633nm radiation was used for excitation and the laser power at the sample position was 2.4 mW. The scattering light was collected by a 10× objective lens (NA = 0.40) to the CCD. All the SERS spectra here were the result of a 60 s accumulation, if without specific description. SERS/fluorescence imaging was performed using the same confocal microscope with a 60× objective lens (NA = 1.35). Actually, in the experiments, the excitation wavelength at 458 nm was used for the fluorescence imaging of NBD while 488 nm and 543 nm were employed for the fluorescence imaging of DOX/Lyso-Tracker Green and DiI/Lyso-Tracker Red, respectively. Meanwhile, the

excitation power at the sample position was ~10 μW. All fluorescence images were the result of an exposure time of 13.867 s with one-way scanning mode, in which the imaging time was 20 ms/pixel. The imaging resolution for x/y and z axes were ~0.2 μm and ~1.4 μm, respectively. SERS imaging was conducted with a 633 nm laser for excitation and the laser power at the sample position was ~160 μW. SERS images were acquired under one-way scanning mode with an exposure time of 65.853 s (imaging time was 100 ms/pixel). The imaging resolution for x/y and z axes of SERS images were 0.232 μm and 1.442 μm, respectively. PALM/STORM images were acquired using a Zeiss Elyra P.1 microscope equipped with 405 nm (50 mW), 488 nm (100 mW), 561 nm (100 mW) and 640 nm (150 mW) lasers. Fluorescence images were recorded using a 100×/1.46 oil immersion objective and an Andor EMCCD camera (iXon DU897). Imaging data were analyzed using the Zeiss Zen 2012 software.

### Preparation of liposomal nanohybrids

The Au@Ag core-shell nanoparticles were prepared using a sodium citrate reduction method following a previously published protocol [37]. Briefly, boiling solution of HAuCl<sub>4</sub> (0.1 mg, 200 mL) was reduced by trisodium citrate (80 mg, 8 mL) under vigorous stirring, resulting in the formation of bare gold nanoparticles. Then the solution of bare gold nanoparticles was further reduced by trisodium citrate (160 mg, 16 mL), followed by a dropwise addition of AgNO<sub>3</sub> solution (10 mM, 20mL). After cooling, the obtained Au@Ag nanoparticles (5 mL) were functionalized with carboxyl groups by an overnight incubation with MMTAA (10 mM, 10 μL) at room temperature. Following the reaction, the Au@Ag@MMTAA nanoparticle suspension was washed twice using centrifugation (3300 rcf, 30 min) and then suspended in deionized water.

Amino-modified liposomes consisting of DSPE-PEG2000-NH<sub>2</sub> were prepared via the standard film hydration method [38]. Briefly, DPPC, DSPE-PEG2000-NH<sub>2</sub> and Chol (55:5:40, m/m) were dissolved in chloroform (5 mg/mL) and evaporated to a thin film under a reduced pressure at 55 °C using a rotary evaporator. For the experiments in which the cellular distribution of liposomes was inspected, 1 mol% of PE-NBD was also included in the mixture to serve as the fluorescent probe. The thin film was further dried under vacuum to remove the trace solvent. The resulting lipid film was hydrated by a gentle shaking with PBS (pH 7.4, 10 mM) or citrate-phosphate buffer at pH 4.0 if doxorubicin loading was intended. The generated multilamellar vesicles (MLV) were sonicated to produce unilamellar

vesicles (ULV). DOX was loaded into the obtained liposomes by the pH gradient method as described elsewhere [26]. The pH value of the liposome suspension was adjusted from 4.0 to 7.4 by dropwise addition of a 10 M stock solution of NaOH. Subsequently, doxorubicin was added to the liposomal dispersion to achieve a drug to lipid ratio of 1:20 (w/w). The loading process was carried out at 55 °C for 30 min. Unencapsulated DOX was removed by ultrafiltration.

To prepare the liposomal nanohybrids, carboxyl Au@Ag@MMTAA nanoparticles (1 mL) and amino liposomes (400 µL) were covalently linked by EDC (10 mM, 5 µL) and NHS (20 mM, 5 µL) at room temperature for 8 h. Free liposomes or nanoparticles in the mixture were removed by a 10 min centrifugation at 2000 ×g. The sediment was dispersed in PBS.

### Liposomal nanohybrids release studies

The drug encapsulation efficiency (EE, defined as the ratio of encapsulated DOX versus the whole amount) was quantified by subtracting the amount of DOX removed through ultrafiltration. For 100% release of the drug, the liposomes or nanohybrids were added to Triton X-100 and sonicated for 3 min (final concentration 0.1%). The encapsulation efficiency of DOX was determined by fluorescence measurement ( $\lambda_{ex}$  = 488 nm and  $\lambda_{em}$  = 580 nm), which can be calculated as follows:

$$EE = 100\% \times F_{\text{encapsulated}} / (F_{\text{encapsulated}} + F_{\text{removed}})$$

Where  $F_{\text{encapsulated}}$  is the fluorescence of Triton X-100 treated samples, and  $F_{\text{removed}}$  is the fluorescence of the filtrate.

In order to monitor its release profile, DOX in the liposomes or nanohybrids was released at different temperatures, and the DOX release percentage from liposomes or nanohybrids was calculated as follows:

$$\% \text{ release} = 100\% \times (F_t - F_0) / (F_{100} - F_0)$$

Where  $F_t$  is the fluorescence at time point  $t$ ,  $F_0$  is the initial fluorescence of the buffer solutions at the start, and  $F_{100}$  is the fluorescence of Triton X-100 treated samples. Variation of DOX released as a function of temperature and a release curve at different time intervals were obtained.

Light-induced DOX release was performed by a pulsed irradiation with 808 nm wavelength NIR light (500 mW) for 120 min at room temperature. After each irradiation, the DOX released from the liposomes or nanohybrids was determined using fluorescence measurement, and the DOX release percentage were calculated using the above equations.

### Stability of liposomal nanohybrids in serum free culture medium

To investigate the stability of the liposomal nanohybrids in the culture medium without 10% FBS, the liposomal nanohybrids were mixed with 1640 medium (volume ratio nanohybrids solution : culture media = 1:4) and incubated for 12 h at 37 °C. The characterization of the nanohybrids was completed and no degradation was observed.

### Cell culture and nanohybrids treatment

Human breast cancer cells (SKBR3) were purchased from China Type Culture Collection and cultured in 1640 medium under a standard cell culture condition (5% CO<sub>2</sub>, 37 °C). Medium was supplemented with 10% fetal bovine serum (Biochrom) and 1% penicillin-streptomycin (Nanjing KeyGen Biotech. Co., Ltd.).

To examine the SERS performance of the liposomal nanohybrids inside living cells, SKBR3 cells were seeded into culture dishes (Corning) and incubated for 24 h. Then, the nanohybrids were added to the cell culture dish (volume ratio nanohybrids solution: culture media = 1:4). Four hours later, the culture media was discarded and the culture dish was gently washed with PBS before the SERS measurement.

To visualize their intracellular stability, nanohybrids were additionally labeled with DiI. These SERS-fluorescence dual labeled nanohybrids were added to the SKBR3 cells and incubated for different time periods. Following the same rinsing with PBS, the cells were imaged under a confocal scanning microscope.

For internalization studies, SKBR3 cells were pretreated with cellular uptake inhibitors for 2 h and then incubated with the liposomal nanohybrids for 4 h at 37 °C. To inhibit clathrin-dependent endocytosis, cells were pre-treated with chlorpromazine (10 µg/mL) [39]. Caveolae-dependent endocytosis was disrupted by pre-treating the cells with nystatin (50 µg/mL) and macropinocytosis was inhibited with cytochalasin D (10 µg/mL) [40]. The impact of temperature on the cellular internalization of nanohybrids was investigated by pre-incubating SKBR3 cells at 4 °C for 2 h prior to the incubation with the liposomal nanohybrids for 4 h. All experiments were conducted in serum-free media. After the pretreatment and incubation, cells were washed thrice with PBS and analyzed by confocal microscopy.

To examine their intracellular fate, the liposomal nanohybrids were added to the SKBR3 cells and incubated for different time periods. Before SERS and fluorescence measurements, the membrane and late endosomes/lysosomes were stained with DiI and

Lyso-Tracker, respectively. Then the culture media were discarded and the culture dishes were gently washed with PBS solution three times. After visualization under a confocal microscope, colocalization analysis was utilized to seek for its intracellular fate. As a control, the same experiments were conducted with pure Au@Ag@MMTAA nanoparticles and liposomes, respectively.

For the photothermal release *in vitro*, SKBR3 cells were treated with nanohybrids for 4 h before the irradiation experiment. After irradiated for 20 min by NIR laser, the degree of drug release was imaged in comparison with cells without irradiation.

Cell viability (MTT assays) was measured as follows. The viability of SKBR3 cells was examined by the MTT (3-(4,5-dimethylthiazol-2-yl)-2,5-diphenyltetrazolium bromide) assay. SKBR3 cells ( $10^4$  mL<sup>-1</sup>) were seeded onto 96-well plates (100  $\mu$ L per well) and incubated for 24 h at 37°C under a 5% CO<sub>2</sub> atmosphere. The following treatment groups were performed: no treatment, NIR laser alone (20 min irradiation), nanohybrids alone and nanohybrids with laser (20 min irradiation). For the treatment with nanohybrids, cells were incubated with particles at 37 °C for 4 h. Thereafter, cells were washed three times with PBS to remove the unbound particles. Cells were then resupplied with 1640 containing 10% FBS. Cells were irradiated with a NIR laser (808 nm) and then incubated at 37 °C for 12 h. After that, 50  $\mu$ L of MTT solution (MTT buffer to dilution buffer 1:4) was added into each well, and the plate was incubated for another 4 h. The reaction was terminated by adding 150  $\mu$ L of DMSO after removing the supernatant medium. When the purple formazan crystals were dissolved by DMSO, the absorbance of the wells at 490 nm was measured with a microplate reader (Bio-Rad model 680). Cells incubated in the absence of hybrids were used as a control for the photothermal cytotoxicity study.

### Statistics analysis

In the cell experiment, one SERS spectrum was collected in each cell, and the measured SERS spectra of 10 cells were used to obtain an average SERS spectrum. Fluorescence and SERS images were analyzed using ImageJ software. For signal intensity, the integrated intensity was measured directly and the total cell numbers were counted manually. The mean signal intensity per cell on a cell image was obtained by dividing the integrated intensity by the cell numbers. The signal average and standard deviation were calculated from 10 cell images. To quantify the colocalization ratio of two signals, the Mander's coefficients indicating the percentage of green signals colocalized with red signals in merged

images was calculated based on analysis of 10 randomly selected regions.

### Abbreviations

Chol: cholesterol; CPZ: chlorpromazine; Cyto-D: cytochalasin D; DDS: drug delivery systems; DiI: 1,1'-dioctadecyl-3,3',3'-tetra-methylindocarbocyanin e; DLS: dynamic light scattering; DOX: doxorubicin; DPPC: 1,2-dipalmitoyl-sn-glycero-3-phosphocholine; DSPE-PEG2000-NH<sub>2</sub>: 1,2-distearoyl-sn-glycero-3-phosphoethanolamine-N-[amino(polyethyleneglycol)-2000] (ammonium salt); EDC: 1-ethyl-3-(3-dimethylaminopropyl)carbodiimide; EE: encapsulation efficiency; EF: enhancement factor; MLV: multilamellar vesicles; MMTAA: 2-mercapto-4-methyl-5-thiazoleacetic acid; MTT: (3-(4,5-dimethylthiazol-2-yl)-2,5-diphenyltetrazolium bromide); NHS: N-hydroxysuccinimide; Nys: nystatin; PBS: phosphate buffered saline; PE-NBD: 1,2-dipalmitoyl-sn-glycero-3-phosphoethanolamine-N-(7-nitro-2-1,3-benzoxadiazol-4-yl) (ammonium salt); SERS: surface-enhanced Raman scattering; TEM: transmission electron microscopy; ULV: unilamellar vesicles.

### Supplementary Material

Supplementary figures.

<http://www.thno.org/v08p0941s1.pdf>

### Acknowledgment

This work was supported by the National Key Basic Research Program of China (Grant No. 2015CB352002), the Natural Science Foundation of China (NSFC) (Grant No.61535003, 61675042, 11374048 and 61605027), the Excellent Youth Foundation of Jiangsu Province (BK20140023), the Natural Science Foundation of Jiangsu Province (BK20140635), the Scientific Research Foundation of Graduate School of Southeast University (YBJJ1555), the Scientific Innovation Research Foundation of College Graduate in Jiangsu Province (KYLX\_0128), the Fundamental Research Funds for the Central Universities.

### Competing Interests

The authors have declared that no competing interest exists.

### References

1. Torchilin VP. Multifunctional, Stimuli-Sensitive Nanoparticulate Systems for Drug Delivery. *Nat Rev Drug Discov.* 2014; 13: 813-27.
2. Laechelt U, Wagner E. Nucleic Acid Therapeutics Using Polyplexes: A Journey of 50 Years (and Beyond). *Chem Rev.* 2015; 115: 11043-78.
3. Chen Y, Gao DY, Huang L. In vivo delivery of miRNAs for cancer therapy: Challenges and strategies. *Adv Drug Deliv Rev.* 2015; 81: 128-41.
4. Pattni BS, Chupin VV, Torchilin VP. New Developments in Liposomal Drug Delivery. *Chem Rev.* 2015; 115: 10938-66.

5. Yan L, Crayton SH, Thawani JP, Amirshaghghi A, Tsourkas A, Cheng Z. A pH-Responsive Drug-Delivery Platform Based on Glycol Chitosan-Coated Liposomes. *Small*. 2015; 11: 4870-4.
6. Guo P, Yang J, Jia D, Moses MA, Auguste DT. ICAM-1-Targeted, Lcn2 siRNA-Encapsulating Liposomes are Potent Anti-angiogenic Agents for Triple Negative Breast Cancer. *Theranostics*. 2016; 6: 1-13.
7. Lei GH, MacDonald RC. Lipid Bilayer Vesicle Fusion: Intermediates Captured by High-Speed Microfluorescence Spectroscopy. *Biophys J*. 2003; 85: 1585-99.
8. Zhang LF, Granick S. How to stabilize phospholipid liposomes (using nanoparticles). *Nano Lett*. 2006; 6: 694-8.
9. Zhang LF, Hong L, Yu Y, Bae SC, Granick S. Nanoparticle-Assisted Surface Immobilization of Phospholipid Liposomes. *J Am Chem Soc*. 2006; 128: 9026-7.
10. Yu Y, Anthony SM, Zhang LF, Bae SC, Granick S. Cationic Nanoparticles Stabilize Zwitterionic Liposomes Better than Anionic Ones. *J Phys Chem C*. 2007; 111: 8233-6.
11. Di Corato R, Bealle G, Kolosnjaj-Tabi J, Espinosa A, Clement O, Silva AKA, et al. Combining Magnetic Hyperthermia and Photodynamic Therapy for Tumor Ablation with Photoresponsive Magnetic Liposomes. *ACS Nano*. 2015; 9: 2904-16.
12. Zhou J, Wang QX, Zhang CY. Liposome-Quantum Dot Complexes Enable Multiplexed Detection of Attomolar DNAs without Target Amplification. *J Am Chem Soc*. 2013; 135: 2056-9.
13. Rengan AK, Bukhari AB, Pradhan A, Malhotra R, Banerjee R, Srivastava R, et al. In Vivo Analysis of Biodegradable Liposome Gold Nanoparticles as Efficient Agents for Photothermal Therapy of Cancer. *Nano Lett*. 2015; 15: 842-8.
14. Smith BR, Gambhir SS. Nanomaterials for In Vivo Imaging. *Chem Rev*. 2017; 117: 901-86.
15. Kumar A, Kim S, Nam JM. Plasmonically Engineered Nanoprobes for Biomedical Applications. *J Am Chem Soc*. 2016; 138: 14509-25.
16. Kwon HJ, Byeon Y, Jeon HN, Cho SH, Han HD, Shin BC. Gold Cluster-Labeled Thermosensitive Liposomes Enhance Triggered Drug Release in the Tumor Microenvironment by a Photothermal Effect. *J Control Release*. 2015; 216: 132-9.
17. Liu Y, Zhang X, Liu Z, Wang L, Luo L, Wang M, et al. Gold Nanoshell-Based Betulinic Acid Liposomes for Synergistic Chemo-Photothermal Therapy. *Nanomedicine*. 2017; 13: 1891-900.
18. Liu Y, Yang F, Yuan C, Li M, Wang T, Chen B, et al. Magnetic Nanoliposomes as in Situ Microbubble Bombers for Multimodality Image-Guided Cancer Theranostics. *ACS Nano*. 2017; 11: 1509-19.
19. Kethineedi VR, Crivat G, Tarr MA, Rosenzweig Z. Quantum dot-NBD-liposome luminescent probes for monitoring phospholipase A(2) activity. *Anal Bioanal Chem*. 2013; 405: 9729-37.
20. Woodle MC, Lasic DD. Sterically Stabilized Liposomes. *Biochim Biophys Acta*. 1992; 1113: 171-99.
21. Roux E, Passirani C, Scheffold S, Benoit JP, Leroux JC. Serum-Stable and Long-Circulating, PEGylated, pH-Sensitive Liposomes. *J Control Release*. 2004; 94: 447-51.
22. Alkilany AM, Abulateefeh SR, Mills KK, Yaseen AIB, Hamaly MA, Alkhatib HS, et al. Colloidal Stability of Citrate and Mercaptoacetic Acid Capped Gold Nanoparticles upon Lyophilization: Effect of Capping Ligand Attachment and Type of Cryoprotectants. *Langmuir*. 2014; 30: 13799-808.
23. Rao W, Wang D, Kups T, Baradacs E, Parditka B, Erdelyi Z, et al. Nanoporous Gold Nanoparticles and Au/Al<sub>2</sub>O<sub>3</sub> Hybrid Nanoparticles with Large Tunability of Plasmonic Properties. *ACS Appl Mater Interfaces*. 2017; 9: 6273-81.
24. Rozic B, Fresnais J, Molinaro C, Calxte J, Umadevi S, Lau-Truong S, et al. Oriented Gold Nanorods and Gold Nanorod Chains within Smectic Liquid Crystal Topological Defects. *ACS Nano*. 2017; 11: 6728-38.
25. Cameron DG, Casal HL, Mantsch HH. Characterization of the Pretransition in 1,2-Dipalmitoyl-sn-Glycero-3-Phosphocholine by Fourier-Transform Infrared Spectroscopy. *Biochemistry*. 1980; 19: 3665-72.
26. Tagami T, Ernsting MJ, Li S-D. Optimization of a novel and improved thermosensitive liposome formulated with DPPC and a Brij surfactant using a robust in vitro system. *J Control Release*. 2011; 154: 290-7.
27. Leung SJ, Kachur XM, Bobnick MC, Romanowski M. Wavelength-Selective Light-Induced Release from Plasmon Resonant Liposomes. *Adv Funct Mater*. 2011; 21: 1113-21.
28. Podstawka E, Kudelski A, Olszewski TK, Boduszek B. Surface-Enhanced Raman Scattering Studies on the Interaction of Phosphonate Derivatives. *J Phys Chem B*. 2009; 113: 10035-42.
29. Woods R, Hope GA, Watling K. A SERS Spectroelectrochemical Investigation of the Interaction of 2-Mercaptobenzothiazole with Copper, Silver and Gold surfaces. *J Appl Electrochem*. 2000; 30: 1209-22.
30. Koo KM, Wee EJH, Mainwaring PN, Wang Y, Trau M. Toward Precision Medicine: A Cancer Molecular Subtyping Nano-Strategy for RNA Biomarkers in Tumor and Urine. *Small*. 2016; 12: 6233-42.
31. Monopoli MP, Aberg C, Salvati A, Dawson KA. Biomolecular Coronas Provide the Biological Identity of Nanosized Materials. *Nat Nanotech*. 2012; 7: 779-86.
32. Lundqvist M, Stigler J, Cedervall T, Berggard T, Flanagan MB, Lynch I, et al. The Evolution of the Protein Corona around Nanoparticles: A Test Study. *ACS Nano*. 2011; 5: 7503-9.
33. Karakoti AS, Das S, Thevuthasan S, Seal S. PEGylated Inorganic Nanoparticles. *Angew Chem Int Ed Engl*. 2011; 50: 1980-94.
34. Oh N, Park J-H. Endocytosis and Exocytosis of Nanoparticles in Mammalian Cells. *Int J Nanomed*. 2014; 9: 51-63.
35. Canton I, Battaglia G. Endocytosis at the Nanoscale. *Chem Soc Rev*. 2012; 41: 2718-39.
36. Tian T, Zhu YL, Zhou YY, Liang GF, Wang YY, Hu FH, et al. Exosome Uptake through Clathrin-mediated Endocytosis and Macropinocytosis and Mediating miR-21 Delivery. *J Biol Chem*. 2014; 289: 22258-67.
37. Zhao L, Shingaya Y, Tomimoto H, Huang Q, Nakayama T. Functionalized Carbon Nanotubes for pH Sensors Based on SERS. *J Mater Chem*. 2008; 18: 4759-61.
38. Weng KC, Noble CO, Papahadjopoulos-Sternberg B, Chen FF, Drummond DC, Kirpotin DB, et al. Targeted Tumor Cell Internalization and Imaging of Multifunctional Quantum Dot-Conjugated Immunoliposomes in vitro and in vivo. *Nano Lett*. 2008; 8: 2851-7.
39. Lacerda L, Russier J, Pastorin G, Antonia Herrero M, Venturelli E, Dumortier H, et al. Translocation Mechanisms of Chemically Functionalised Carbon Nanotubes Across Plasma Membranes. *Biomaterials*. 2012; 33: 3334-43.
40. Sarker SR, Hokama R, Takeoka S. Intracellular Delivery of Universal Proteins Using a Lysine Headgroup Containing Cationic Liposomes: Deciphering the Uptake Mechanism. *Mol Pharm*. 2014; 11: 164-74.